Nitride-bonded silicon nitride from slip-cast Si + Si_3N_4 compacts

R. Ramachandra Rao and T.S. Kannan
Materials Science Division, National Aerospace Laboratories, Bangalore, 560 017 India

(Received 22 November 2000; accepted 19 November 2001)

The dispersability of Si and Si_3N_4 powders in aqueous media was monitored by particle-size distribution, sedimentation behavior, viscosity/rheological studies, and electrokinetic behavior [zeta potential (ZP) analysis] as a function of pH of their slips. The pH values of 4 and 8 for Si and 10 for Si_3N_4 resulted in optimum dispersion, characterized by minimum in sedimentation height, minimum in viscosity, and maximum in ZP. The optimum slips of Si + Si_3N_4 mixtures conditioned in the pH range 8 to 10 were slip cast to obtain green compacts having a density in the range of 59% to 66% theoretical value. When nitrided, these compacts yielded nitride-bonded Si_3N_4 products having a density of 2.06 to 2.28 g cm^{-3}, Si_3N_4 bonding phase of 20–60%, and 3-point flexural strength values in the range of 50 to 150 MPa. The microstructure consisted of very fine particles as well as fibrous or whiskerlike α–Si_3N_4 binding phase enveloping the matrix Si_3N_4, in total consisting of 90% α–Si_3N_4 and the rest being β–Si_3N_4 phase.

I. INTRODUCTION

Silicon nitride (Si_3N_4) ceramics have been recognized as potential candidates for high temperature, wear, and structural applications, e.g., in heat engine parts (diesel and gas turbine), in heat exchangers, in friction and wear-resistant components (bearings), and as cutting tools. Si_3N_4 exhibits superior mechanical (strength and hardness) and chemical (oxidation and corrosion resistance) properties as well as thermal stability at high temperatures.[1–4] Among the two major types of Si_3N_4 products, namely, dense sintered Si_3N_4 (obtained by sintering, hot pressing, hot isostatic pressing, etc., of Si_3N_4 powder), and the porous reaction bonded silicon nitride (RBSN) obtained by reactive nitridation of silicon, the later has attracted the attention of ceramic researchers during the last 3–4 decades because of its near net-shape forming capability as well as its lower production costs.[3–6] This process has two main drawbacks because it requires longer nitriding times (20–100 h), especially for thicker samples, and considerably larger amounts of porosity (10–20%), apparently retained in the structure that degrades their strength, toughness, and oxidation resistance at higher temperatures. To overcome these problems, two interesting approaches to Si_3N_4 product development have been followed. One is the nitridation of Si compacts containing various amounts of Si_3N_4 as inert filler, which reduces the nitridation time. In another approach, the post sintering of a RBSN product containing appropriate sintering aids has been followed to improve density by minimizing the large volume shrinkage associated with the sintering of Si_3N_4 powder compacts. The later approach also lowers the production costs associated with the machining process.[4,7,8]

Focusing on the first approach of the nitriding of Si containing Si_3N_4 as an inert secondary phase, very few investigations are presented in the open literature.[7–15] Pompe *et al.*[8] and Falk *et al.*[9,10] extensively studied the nitridation of cold isostatically pressed cold isostatic pressing (CIP) compacts of coarse ($\leqslant$300 μm) Si containing 30 to 50 wt.% of fine (approximately 0.6 μm) Si_3N_4. They observed that the inert α–Si_3N_4 act as the filler and increases the rate of nitridation. The nitrided product has high machinability with 3-point flexural strength of 120–140 MPa and high α-phase at lower nitridation temperatures ($\leqslant$1350 °C). The presence of sintering additives like Y_2O_3 and Al_2O_3 increased the nitridation kinetics forming both α– and β–Si_3N_4 phases with the later predominantly at higher temperatures ($\geqslant$1350 °C). Sintering at 1850 °C converts all α–Si_3N_4 form into β-form by Ostwald ripening mechanism. Atkinson *et al.*[11] has shown that up to 50% Si_3N_4 filler addition serves the dual purpose of seeding and providing open pore structure during nitridation, which favors α–Si_3N_4 formation due to vapor-phase reaction mechanism. The seeding helps in controlling the α/β-ratio formation, extent of reaction, and final density achieved. Gregory and Richman[12] investigated the role of Si_3N_4 additions ($\geqslant$30 wt.% with various α- to β- ratios) on the reaction bonding of Si compacts prepared by CIP. The important observation made is that the Si_3N_4

particles added to the starting silicon have a seeding effect such that the percentage of α–Si_3N_4 phase in the final product formed was proportional to the percentage of α–Si_3N_4 present in the seeded material. This is attributed to providing a higher number of growth sites for α–nitride formation as well as providing an open pore network and nitriding conditions favorable for α-formation (gas phase reactions).

Williams *et al.*[7,13] investigated the effect of α–Si_3N_4 grog additions (0–16 wt.%) on the slip casting of Si and its nitridation using a nitrogen demand cycle experiment with 20.7 Kpa N_2 gas containing 4% H_2 as a nitridation accelerator and 25% He as a thermal equilibrator. The Si_3N_4 grog progressively lowered the cast density and permitted greater nitridation of a given section and complete nitriding of thicker sections. The open pore structure of the grog-containing mixes favored low-temperature vapor-phase reactions resulting in a higher percent α–Si_3N_4 than β–Si_3N_4 in the mixture, the later forming at higher temperatures by vapor-liquid-solid (VLS) mechanism in the presence of a liquid ($FeSi_x$ eutectic) phase. The grog additions consistently lowered the densities, the room and high-temperature strengths, and resistance to oxidation. The microstructure of the product surfaces showed mats of long fibrous crystals and occasional blocky inclusions of α–Si_3N_4 and amorphous Si_3N_4 while fibrous as well as short elongated needlelike crystals of α–Si_3N_4 were found inside the pores of a fractured specimen. Huang *et al.*[14] studied the effects of pore-size distribution on the nitridation kinetics of Si compacts containing 0–40 wt.% of Si_3N_4 prepared by CIP using flowing gas mixtures of 4% H_2, 21% He, and 75% N_2. Samples having a higher pore volume and a larger pore diameter reacted faster at lower temperatures and showed higher weight gain and less residual silicon. Samples displayed decreasing initial nitridation with increasing silicon nitride content (decrease in pore volume) below 1200 °C, while beyond 1200 °C the reactions averaged out due to closure of the pores with the Si_3N_4 formation. Bhat and Roy[15] studied the nitridation of Si in the Si_3N_4–Si system where Si_3N_4 (93% α- and 7% β-phases) is the major component (60, 80, 90 wt.%) in comparison with 100% of Si, at temperatures of 1200 to 1400 °C for 4–48 h under flowing nitrogen. The presence of α–Si_3N_4 in the Si + Si_3N_4 compacts favored faster nitridation at all temperatures and an increased amount of α–Si_3N_4 at all compositions. Eighty-eight percent of α–Si_3N_4 and 12% of β–Si_3N_4 was formed in the products from compacts of 60 Si_3N_4 + 40Si as compared to 68% of α–Si_3N_4 and 32% of β–Si_3N_4 from 100% Si compacts.

The authors have agreed that the presence of a higher percentage of oxidized surfaces on the added Si_3N_4 and overall dilution of the presence of the total iron impurity in silicon (by Si_3N_4 addition) favored the formation of α–Si_3N_4 in preference to β–Si_3N_4, which forms by VLS mechanism in the $FeSi_x$ eutectic in the case of nitridation of pure silicon. The predominant formation of α–Si_3N_4 is revealed clearly by x-ray diffraction (XRD) patterns of the nitrided products of the Si + Si_3N_4 mixtures.

Because of the significant importance of the Si_3N_4 ceramics and the scanty literature available on the self-bonding process for the production of Si_3N_4, the nitridation of Si–Si_3N_4 compacts having 15–50 wt.% of Si has been investigated in this study. This has led to the formation of nitride-bonded silicon nitride (NBSN) or self-bonded silicon nitride (SBSN) products. The slip-casting route has been employed to produce the green compacts of the above systems starting from colloidally processed, optimally dispersed slips, as this method has not been well exploited despite all the known advantages of colloidal processing.

II. EXPERIMENTAL

Commercial Silicon (Si) powders (Types HQ and RQ, Kema Nord Industries, Norway) and Si_3N_4 powder (Type HCST–S1, Hermann C. Starck, Germany) were used in this study. The powders were characterized for phase purity by XRD (x-ray diffractometer, PM 9002, Phillips, Holland, The Netherlands) and for their specific gravity by helium gas pyknometry (Multivolume Pyknometer, 1305, Micromeritics, Norcross, GA). The dispersability of these powders in deionized water (DIW) as a function of pH was investigated by using various experimental techniques like particle/floc-size distribution, ZP (zeta potential) measurements, sedimentation studies, viscosity, and rheological behaviors. The experimental details and the results of such studies were presented elsewere.[16,17] For slurry characterization, the powders were dispersed in DIW with continuous magnetic stirring for 5–20 min depending upon the required total solid loading (in the range 5–50 wt.%). The pH of the slurry was adjusted to various values ranging from 2 to 12 using HNO_3 (70% sol.) for acidic and NH_4OH (25% sol.) for basic ranges, respectively.

The particle/floc-size distribution of the powders in DIW (5 wt.%) as a function of pH was determined using an x-ray sedimentation technique (Sedigraph 5100, Micromeritics, Norcross, GA). The sedimentation behavior of the 20 wt.% solid loaded slurries (4 g in 15 cm^3 of DIW) maintained at different pH values (2–11) in long test tubes of uniform dimension (150 mm × 13 mm φ) was studied to arrive at the condition of best dispersion. The height of the solid sediment was measured from the bottom of the test tube as a function of time and plotted as a function of pH. The viscosity of 52 wt.% Si slips and 44 wt.% Si_3N_4 slips were measured at different shear rates in the range 500 to 2000 S^{-1} as a function of pH of the slurry by using a rotational viscometer (Viscotester

VT500, Haake, Germany). The electrophoretic mobility and hence the ZP of Si and Si_3N_4 particles in 20 wt.% solid loaded slurries were measured as a function of pH using a mass transport apparatus (ZP analyzer, 1202, Micromeritics, Norcross, GA).

Aqueous slips of Si + Si_3N_4 mixtures (in the ratios of 0 + 100, 15 + 85, 25 + 75, 50 + 50, 75 + 25, 85 + 15, and 100 + 0 wt.%, respectively) were prepared by dispersing the required quantity of two powders simultaneously into DIW using a magnetic stirrer. The pH of the slip was adjusted to a value between 8 and 10 based on the optimum dispersion condition achieved from slurry characterization studies done on Si and Si_3N_4 powders separately. The resulting slips were milled in polythene jars for about 16 to 20 h using Al_2O_3 balls as milling media. In each composition of Si + Si_3N_4, initially about 50 to 55 wt.% solid-loaded slips could be prepared by dispersing both Si and Si_3N_4 simultaneously and by the intermediate addition of fresh powder mixtures of Si + Si_3N_4 an enhanced final solid loading of 72 wt.% (with respect to Si + Si_3N_4) was achieved. The slip was then cast into plaster molds to obtain bar [50 × (9–10) × (8–9) mm^3] and disc (25 mm φ × 10 mm) shaped specimens. Similar aqueous slips of Si + Si_3N_4 mixtures containing 25 and 50 wt.% of Si (balance being Si_3N_4) and 1 wt.% of Fe_2O_3 (with respect to Si) were also made and slip-cast. The green densities of the slip-cast compacts were derived from their weight and dimensional (volume) measurements.

The slip-cast bodies of Si + Si_3N_4 mixtures were nitrided in the temperature range of 1400 to 1500 °C for various periods ranging from 2–4 h in a resistive graphite furnace (Dynatech Engineering, Mumbai, India), under a constant static positive pressure (0.18 MPa) of high-purity nitrogen (Grade I, Bhoruka Gases, Bangalore, having a maximum impurity level of 8 ppm). The nitrided products were characterized by their: (i) percentage of nitridation, (ii) percentage of Si_3N_4 bond formed (both derived from sample's weight gain after nitridation), (iii) the nitrided density (from weight and volume measurements of the nitrided products), and (iv) apparent porosity (by water displacement method). The different crystallographic phases formed due to nitridation were analyzed through their x-ray diffractograms. The 3-point flexural strengths were measured for rectangular bar specimens (50 × 8–10 × 8–9mm^3) using a span width of 40mm and crosshead speed of 0.5 $mm.min^{-1}$ in a Universal Testing Machine (5500R, Instron, High Wycombe, UK). In each case about 10 to 12 samples were used for modulus of rapture testing and standard deviation had been calculated. The microstructures of the fractured surfaces were observed under a scanning electron microscope (Leo 440, Leo Electron Microscopy, Cambridge, UK).

III. RESULTS AND DISCUSSION

A. Slurry characterisation

Some of the physical characteristics of the Si (HQ and RQ) and Si_3N_4 (S1) powders are presented in Table I along with their chemical composition (as provided by the supplier). Figure 1 depicts the particle-size distribution curves at the optimum dispersion condition of pH = 8 for two Si[16] powders and pH = 10 for Si_3N_4[17]. The results of Fig. 1 and Table I indicate that Si_3N_4 particles are relatively finer with d_{10} = 0.42 μm, d_{50} = 0.98 μm, and d_{90} = 2.5 μm as compared to both the Si powders, which have similar particle-size distributions (d_{10} = 0.72 μm, d_{50} = 2.9 μm, and d_{90} = 4.8 μm).

The metallic Si as well as the nonoxide Si_3N_4 powders are usually found to be surface oxidized, and the fine (submicron) particles contain a superficial layer of silica on their outer surfaces.[16–20] When these powders are dispersed in water, the oxidized surfaces get hydrolyzed to form amphoteric silanol (Si–OH) groups.[16,21] In addition, Si_3N_4 particles also contain basic amine groups

TABLE I. Characteristics of Si and Si_3N_4 powders.

Powder type	Supplier	Chemical composition[a] (%)		Phases (XRD)	Density (g cm^{-3})	Particle size (μm)		
						d_{10}	d_{50}	d_{90}
Si HQ & Si RQ	Kema Nord Industries Norway	Si	99.70	Silicon	2.301	0.72	2.90	4.80
		Al	0.08					
		Fe	0.04					
		Ca	0.01					
		Ti	0.001					
Si_3N_4 S1	HCST Germany	N	38.00	α-Si_3N_4 = 92%	3.187	0.42	0.98	2.50
		C	0.30	β-Si_3N_4 = 8%				
		O	2.00					
		Fe	0.10					
		Al	0.10					
		Ca	0.02					
		Free Si	0.30					

[a]As provided by the suppliers.

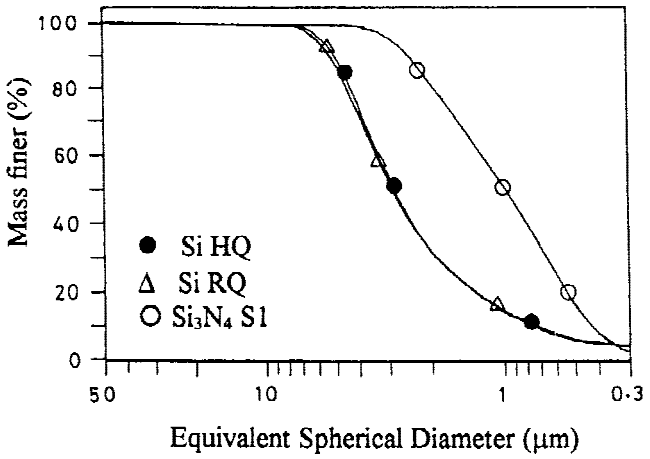

FIG 1. Particle-size distribution curves for, ● = Si HQ and Δ = Si RQ at pH = 8.0 and O = Si_3N_4 S1 at pH = 10.0.

viz. silazane (Si_2–NH) and silylamine (Si–NH_2) on their surfaces.[17,19,20] In aqueous medium the silanol and amine groups undergo acid/base reactions depending on the pH of the medium and develop positive or negative surface charges depending upon the adsorption of either of the potential detemining OH^- or H^+ ions.[16–21]

$$SiOH_2^+ \xleftarrow{H^+} SiOH \xrightarrow{OH^-} SiO^- + H_2O$$

$$SiNH_2 \xleftarrow{H^+} SiNH_3^+$$

$$Si_2NH \xleftarrow{H^+} Si_2NH_2^+$$

These surface charged particles adsorb a layer of opposite charged ions resulting in an electrical double layer and an electrical potential developed at the shear plane between the bound and free liquid and is called the ZP. On close approach, these particles repel each other due to the overlapping of the electrical double layer. This electrostatic repulsion between the charged surfaces of the particles overcomes the van der Waals force of attraction; hence, prevents particle agglomeration and promotes the dispersion of the fine particles in aqueous media. The electrostatic repulsion developed between the powder particles could be modified by adjusting the pH of the medium or by adding specific ionic groups (inorganic or organic) in the form of electrolytes (dispersing agents). The electrical charge density of the surface as well as the surface potential or ZP arising from the adsorption of potential determining ions or ionic groups determines the dispersability of the powder particles in the aqueous medium. Higher ZP, which indicates a higher surface charge on the particles (higher double layer thickness), leads to increased electrostatic repulsion between the particles and hence good dispersion. On the other hand, with lower ZP, the van der Waals forces of attraction may overcome the electrostatic repulsion leading to agglomeration of the particles.

The state of dispersion of Si and Si_3N_4 powders in DIW as a function of pH was manifested in terms of height of the solid sediment from the bottom of the test tube, measured as a function of time (1–24 h), and the results were presented in detail elsewhere.[16,17] Representative plots of the sedimentation heights as a function of pH of the slurry measured after a time interval of 6 h for Si HQ, Si RQ, and Si_3N_4 S1 powders are presented in Fig. 2. A variation in sedimentation heights as a function of pH is attributable to different levels of agglomeration or flocculation of the particles that leads to different levels of packing in free space under the force of gravity. Under the conditions of good dispersion, particles settle into tightly packed sediments (ideal packing) leading to a minimum in sedimentation heights. On the contrary, in a flocculated system, the agglomerated particles fall rapidly under the force of gravity, (larger weight) resulting in loosely packed sediments that leads to larger sedimentation heights. The sediment height is inversely related to the dispersability of the powder; the more dispersed the powder, the smaller the sediment height. From Fig. 2 it can be seen that the two Si (HQ and RQ) powders show a similar state of dispersion with minima in sedimentation heights around two pH regions of 4 to 5 and 8, while the Si_3N_4 powder shows minimum height in the pH range 8.5 to 11.0. This sedimentation behavior for both Si and Si_3N_4 powders show a similar trend at all the times,[16,17] indicating the above pH values as the conditions of optimum dispersion for the respective powders.

The dispersabilty of fine powder particles in a liquid medium can also be correlated to the viscosity of the slips. The viscosity values measured as a function of pH for 52 wt.% Si (HQ and RQ) and 44 wt.% Si_3N_4 S1 slips at a shear rate of 972 s^{-1} presented in Fig. 3 supports the results of sedimentation behavior of these

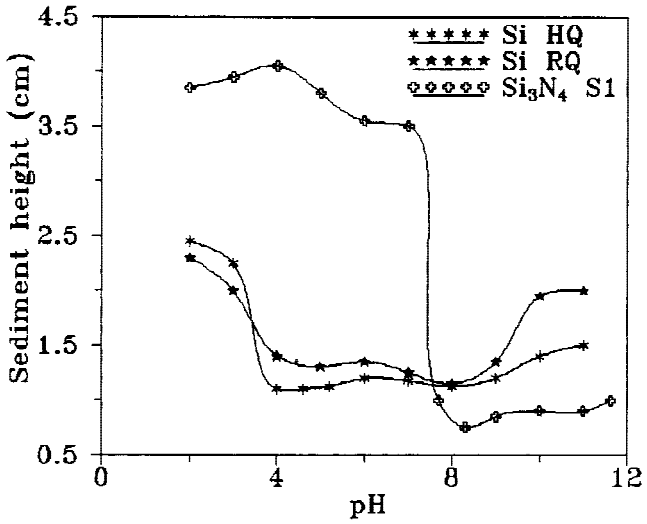

FIG. 2. Sedimentation height as a function of pH for Si (HQ and RQ) and Si_3N_4 S1 after 6 h.

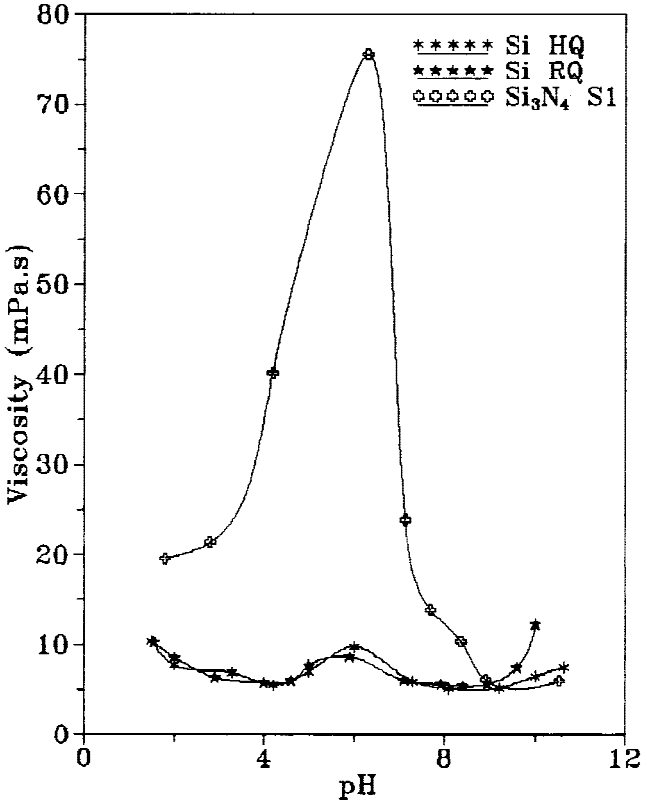

FIG. 3. Viscosity as a function of pH for Si (HQ and RQ) and Si_3N_4 S1 at a shear rate of 972 s^{-1}.

powders. The minimum viscosity observed for Si slips at the pH values of 4 to 5 and 8 and for Si_3N_4 slips at the pH values of 9 to 11 indicates good dispersion of the powder particles. At other pH regions, significant agglomeration of particles coupled with entrapping of liquid in the inter-particulate pore spaces increased the effective solid loading and thereby considerable increase in the slip viscosity.[16,17] When such a slurry is subjected to higher shear stresses, shear thinning flow results due to breakdown of the flocculated structure and release of the entrapped liquid as reported earlier under studies on rheological behavior.[16,17] Similar behavior has also been reported for SiC slurries under studies on rheological behavior.[22] The relatively lower viscosity of Si particles compared to the Si_3N_4 particles in the agglomerated region could be attributed to the coarser and wider particle-size distribution in the case of silicon as well as the difference in surface characteristics of Si and Si_3N_4 powders.

The variation in sedimentation and viscosity behavior of Si and Si_3N_4 slips, representing their state of dispersion, are directly related to the surface charges on their respective particulate surfaces. The ZP arising out of net effective surface charges on the particles in the suspension directly reflects the dispersability levels of the particles in a medium. The ZP measured as a function of pH for Si (HQ and RQ) and Si_3N_4 S1 powders presented in

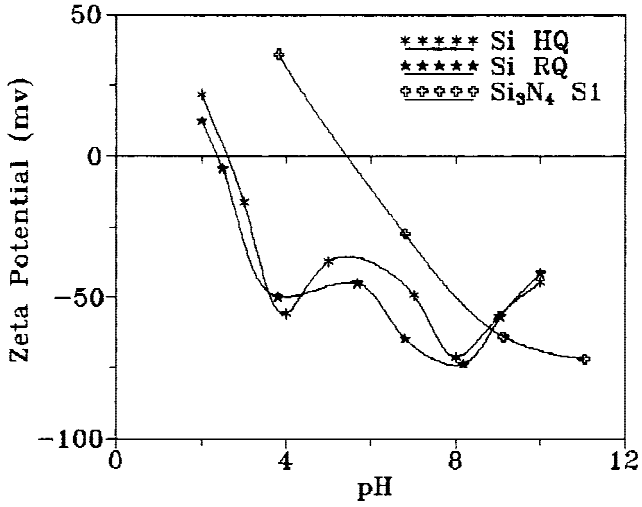

FIG. 4. Zeta potential versus pH curves for Si (HQ and RQ) and Si_3N_4 S1 powders.

Fig. 4 show that Si powders develop higher surface charges in the pH ranges around 4 and 8. Si_3N_4 powders do so around pH values of 9 to 11 indicating these as the pH regions of their optimum dispersion, which is reflected by lower sedimentation heights and minimum viscosity values for their slips. The isoelectric points (IEP) for Si around pH = 2.4 and 2.6 and for Si_3N_4 at pH = 5.4 represents the regions of high agglomeration (due to van der Waals force of attraction) leading to higher sedimentation heights and higher viscosity for the slips. Even though the reason for a slight decrease in ZP values for Si around the pH value of 6 is not currently known, the resulting partial agglomeration of the particles is evidenced by an increase in viscosity values as shown in Fig. 3.

From the results of slurry characterization experiments it can be concluded that the conditions of optimum dispersion for Si are at the pH values of 4 and 8 and for Si_3N_4 it is in the pH region of 9 to 11.

B. Slip casting of Si + Si_3N_4 (0–100 wt.%) mixtures

The different slip-casting compositions and the green density of the slip-cast compacts are presented in Table II. The various samples are identified as xxNBSN or xxNBSNF, where xx = initial amount of Si in wt.%, NBSN = nitride-bonded silicon nitride and F = presence of Fe_2O_3 in the green sample. Thus 0 NBSN refers to the compacts obtained by slip casting only pure Si_3N_4 powder, whereas, 100 NBSN or RBSN refers to the compacts obtained by slip casting only Si powder, which on nitridation results in RBSN. The change in compositional density [calculated from rule of mixture by considering the theoretical density (TD) of Si = 2.23 g cm^{-3} and Si_3N_4 = 3.2 g cm^{-3}], bulk density (by weight and dimensional measurements) and the percentage of TD (with respect to the compositional density of Si + Si_3N_4

mixtures) are plotted in Fig. 5 as a function of the amount of Si present in the Si + Si_3N_4 green compacts without the addition of Fe_2O_3. The green density of slip-cast Si + Si_3N_4 mixtures (0–100 wt.%) is found to decrease with the increase of Si content in correlation with the decrease of compositional density (Table II and Fig. 5). However, the percentage TD (of the Si + Si_3N_4 mixtures) increases with Si content. This reveals the better packing efficiency of Si powder particles as compared to that of Si_3N_4. A similar behavior was observed while slip-casting Si + SiC mixtures[23] to produce NBSC products.

C. Nitridation of slip-cast Si + Si_3N_4 (0–85 wt.%) compacts

Slip-cast Si + Si_3N_4 compacts containing 0 to 85 wt.% of Si_3N_4, without the addition of Fe_2O_3, were nitrided in a graphite furnace under a static positive pressure of high purity nitrogen (0.18MPa) at temperatures of 1450 and 1500 °C for 2 to 4 h. The percentage nitridation and the nitrided density of the products calculated on the basis of weight gained during nitridation are plotted as a function of percentage of initial Si content, the nitridation temperature, and time of nitridation in Figs. 6 and 7, respectively. It could be seen that the percentage nitridation is a function of the percentage of Si present in the compact as well as of temperature and time of nitridation. A considerably lower percentage of nitridation (20–30%) was observed for compositions with higher percentages of Si (50–100%) at 1450 °C for 2 h, which could be considered as an induction period of the nitridation reaction at this temperature. At the higher temperature of 1500 °C, a slightly lower percent of nitridation was observed for compacts containing lesser percentages of Si (15–25%) than that observed at a lower temperature of 1450 °C. This is probably due to loss of some Si by evaporation [may be in the form of SiO(g)] at the higher temperature. The percentage nitridation results of Fig. 6 correlate well with the nitrided density data depicted in Fig. 7. The higher percentage of nitridation at higher temperatures or longer times resulted in higher density products.

The phase analysis of the starting slip-cast green body and the nitrided products has been carried out by XRD (x-ray diffraction) method. The typical XRD spectra for the green compact (25% Si + 75% Si_3N_4) as well as that taken on the surface and at the interior core of a nitrided bar specimen (50 × 8 × 8 mm^3) of 25 NBSN sample, presented in Figs. 8(a)–8(c) reveals the presence of α–Si_3N_4 as the major phase and β–Si_3N_4 as the minor phase. The XRD spectra taken on the surface of the sample [Fig. 8(b)] shows the formation of β–SiC, which is attributed to the high carbon activity (a_c = 1) present inside the furnace as observed in earlier studies for the

TABLE II. Compositions and green density of slip cast Si + Si_3N_4 compacts.

S1. No.	Sample identity	Initial Si content (wt.%)	Initial Si_3N_4 content (wt.%)	Green density ($g\ cm^{-3}$)	Green density (%)$
1	0 NBSN	0	100	1.894	59.2
2	15 NBSN	15	85	1.843	60.1
3	25 NBSN	25	75	1.824	61.1
4	50 NBSN	50	50	1.749	63.3
5	75 NBSN	75	25	1.645	64.6
6	85 NBSN	85	15	1.624	66.0
7	100 NBSN (RBSN)	100	0	1.545	66.3
8	25 NBSNF[a]	25	75	1.763	59.1
9	50 NBSNF[a]	50	50	1.650	59.7

[a]1 wt.% of Fe_2O_3 addition with respect to silicon content.
$ percentage theoretical density with respect to the theoretical density of Si + Si_3N_4 mixtures calculated by the rule of mixtures (Theoretical density for Si = 2.22 g cm^{-3} and for Si_3N_4 = 3.2 g cm^{-3}).

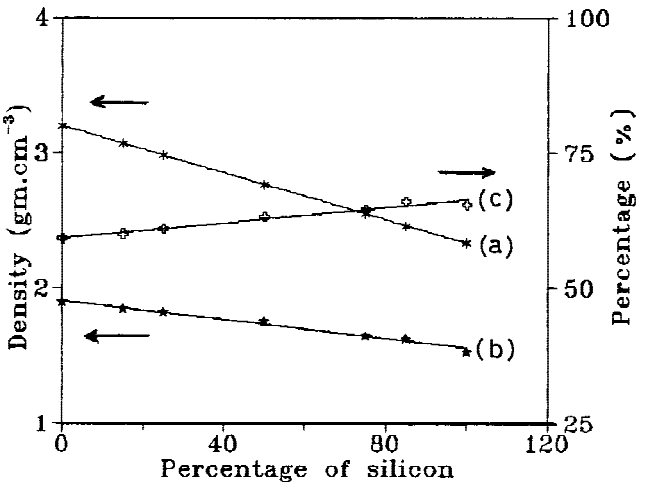

FIG. 5. Change of (a) compositional density, (b) bulk density, and (c) percentage TD of slip-cast Si + Si_3N_4 as a function of percentage of Si in the green compact.

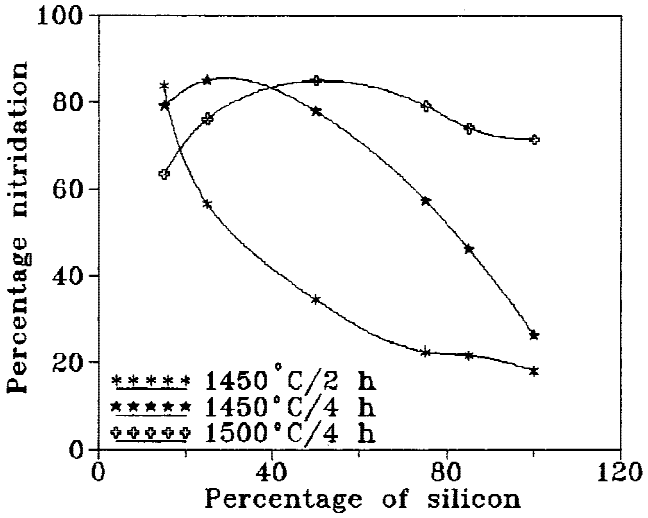

FIG. 6. Percentage nitridation of slip-cast Si + Si_3N_4 compacts as a function of percentage of silicon, nitridation temperature, and time.

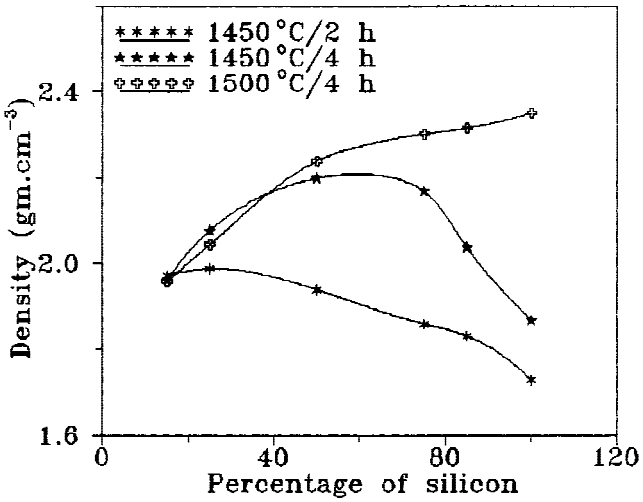

FIG. 7. Nitrided density of slip-cast Si + Si_3N_4 compacts as a function of percentage of silicon, nitridation temperature, and time.

nitridation of pure Si[24] and Si + SiC[23] compacts. Contrary to a large proportion of β−Si_3N_4 formed in RBSN[24] and NBSC[23] products, the interesting feature observed in the case of NBSN compacts of the present study is the higher percentage of α−Si_3N_4 with α− to β−ratio of 90:10 as calculated from the ratio of the highest intensity peaks for α−Si_3N_4 and β−Si_3N_4 (α/β = 9). This is nearly the same as that present in the Si_3N_4 S1 powder (α:β = 92:8) used in the starting composition as revealed from the XRD spectra in Fig 8(a). Another advantage of NBSN formulation is the absence of the Si_2N_2O phase as compared to those of RBSN[24] and NBSC[23]. These findings could be attributed to the seeding effect of α−Si_3N_4 phase present in the slip-cast compacts. Similar observations were made by Williams *et al.*,[7,13] Atkinson *et al.*,[11] Gregory and Richman,[12] and Bhat and Roy[15] on nitridation of Si_3N_4–Si systems. The type of phase distributions observed with all the NBSN samples are similar except that some unreacted free Si could also be seen at the interior core of the samples, which had a higher percentage of Si (≥50%) in the green body; hence, their nitridation was found to be incomplete.

D. Nitridation of Si, 25 wt.% + Si_3N_4, 75 wt.% and Si, 50 wt.% + Si_3N_4, 50 wt.% compacts containing Fe_2O_3

The Si, 25 wt.% + Si_3N_4, 75 wt.%, and Si, 50 wt.% + Si_3N_4, 50 wt.% compacts containing 1 wt.% Fe_2O_3 (with respect to Si) designated as 25 NBSNF and 50 NBSNF were nitrided at 1400 °C for 2 h. The green density, percentage nitridation, the percent of Si_3N_4 bond formed, nitrided density, and the apparent porosity values for the Fe_2O_3 added 25 NBSNF and 50 NBSNF samples are presented in Table III along with the results for 15 NBSN and 25 NBSN samples (without Fe_2O_3) nitrided at higher temperatures of 1450 °C for 2 and 4 h, respectively. This higher nitridation temperature of 1450 °C is used for samples without the Fe_2O_3 addition since the nitridation

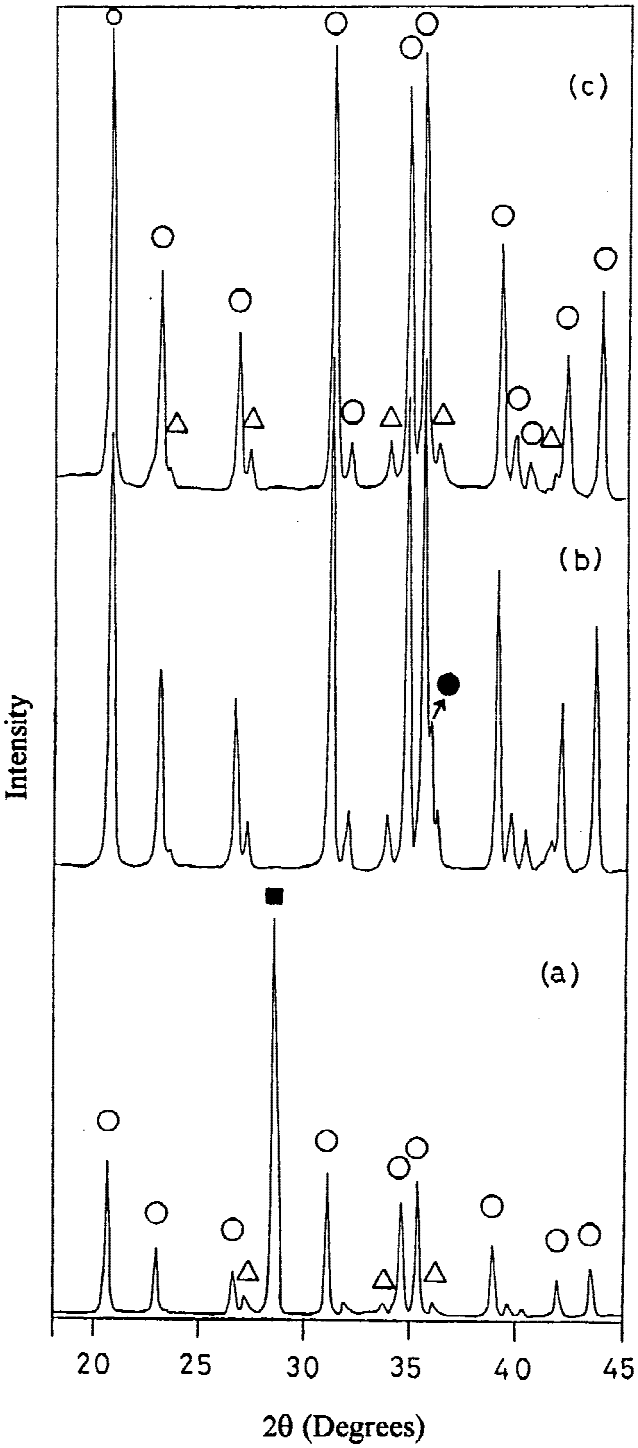

FIG. 8. XRD spectra of 25 NBSN (a) as unreacted slip-cast green compact, (b) on the outer surface, and (c) at the central core of a nitrided bar specimen (50 × 8 × 8 mm^3). Phases identified: O = α–Si_3N_4, Δ = β–Si_3N_4, ● = β–SiC, and ■ = Si.

is not completed at 1400 °C. It has been well established that the Fe_2O_3 will enhance the nitridation by catalytic action through the formation of a low melting iron siliside ($FeSi_x$) compound[7,13,25] and leads to near completion of the nitridation at lower temperatures as well as at shorter times. The 25 NBSNF and 50 NBSNF compositions (with Fe_2O_3) on nitriding at 1400 °C for 2h resulted in 92% and 94% nitridation with nitrided densities of 2.149 and 2.279 g cm^{-3}, respectively, as depicted in Table III. On the contrary, 25 NBSN and 50 NBSN samples (without Fe_2O_3) on nitriding even at a higher temperature of 1450 °C for 2 h resulted in only 57% and 35% nitridation and the nitrided densities of 1.988 and 1.939 g cm^{-3}, respectively, as depicted in Figs. 6 and 7. The density values obtained for 25 NBSNF and 50 NBSNF samples are slightly higher than reported by Bhat and Roy.[15] The XRD spectra taken on the surface as well as on the interior core of a bar specimen ($50 \times 8 \times 8$ mm^3) reveals the presence of about 90% α–Si_3N_4 and 10% β–Si_3N_4 and is in correlation with those obtained for samples without the Fe_2O_3 addition.

E. Mechanical and microstructural characterization of NBSN products

The flexural strength values measured by the 3-point bending method for NBSN bodies obtained from Si + Si_3N_4 compacts containing 15, 25, and 50 wt% of Si in the initial green compacts with or without the addition of Fe_2O_3 are presented in Table III. The increased amount of Si_3N_4 bond formed as well as a slight increase in density and decrease in porosity for compositions with a higher percentage of silicon present in the green compact are responsible for the increase in flexural strength of the NBSN products. The 3-point flexural strength value of 147 ± 34 MPa obtained for 50 NBSNF samples with 60% Si_3N_4 bond is comparable or slightly better than 120–140 MPa reported by Pompe and Hermansson[8] for samples containing higher Si_3N_4 bond phase of 60–80%. These strength values can be considered better because the samples have a slightly lower density of 2.28 g cm^{-3} and high porosity of 26.8% as compared to a higher density of 2.35–2.40 g cm^{-3} for samples reported by Pompe and Hermansson.[8] These higher strength values despite a lower density and higher porosity could be attributed to the uniform and homogeneous microstructures of the green body in which the formation of agglomeration has been prevented through slurry optimization techniques. The flexural strength values in the range of 57 ± 10 to 147 ± 34 MPa are considered promising for nitride-bonded silicon nitride bodies produced by slip casting. These strength values are higher than that obtained for NBSC products (53–120 MPa) containing the same amount of Si_3N_4 bonding (19–57% Si_3N_4 bond) produced by the similar route of slip casting followed by nitridation.[25] This can be attributed to three factors. Firstly, the Si_3N_4 particles used are much finer ($d_{10} = 0.42$ μm, $d_{50} = 0.98$ μm, $d_{90} = 2.50$ μm) than the SiC ($d_{10} = 0.6$ μm, $d_{50} = 2.5$ μm, $d_{90} = 8.0$ μm) particles used in the above experiments. Another factor is the phase homogeneity (mainly α–Si_3N_4) observed in the NBSN products as compared to the multiphase (α–Si_3N_4, β–Si_3N_4, and Si_2N_2O) bond formed in the case of NBSC products.[23,25] The Si_3N_4 matrix phase in the NBSN product can be more reactive than the SiC phase in the NBSC product at the temperature of reaction considered leading to better bonding between the Si_3N_4–Si_3N_4 phase rather than between the Si_3N_4–SiC phase.

Typical scanning electron microscopy (SEM) pictures of the fractured surfaces of the NBSNF products are presented in Figs. 9(a)–9(c). The SEM in Fig. 9(a) showing the fractography of 25 NBSNF sample reveals a microstructure in which very fine particles of newly formed Si_3N_4 bonds the parent Si_3N_4 particles. In Figs. 9(b) and 9(c) some fine fibrous or whiskerlike growth, forming meshlike structures of Si_3N_4 can be observed in the pores, binding the original or newly grown Si_3N_4 particles with blocky morphology. These microstructural features are similar to those reported by Williams and Ezis,[7] Pompe and Hermansson,[8] Falk *et al.,*[9,10] and Bhat and Roy.[15] The fine fiber or whiskerlike grown Si_3N_4 inside the pore structure is probably the α-form as the open pore structure favors the low-temperature vapor-phase reaction leading to the formation of α-Si_3N_4 as predicted by Williams and Ezis.[7] The massive Si_3N_4 matrix with blocky morphology could consist of mainly

TABLE III. Characteristics of Nitride bonded silicon nitride (NBSN) products.

Sample identity	Nitridation temperature/ time (°C/h)	Initial Si content (wt.%)	Green density (%) $	Percent nitridation (%)	Si_3N_4 bond (%)	Nitrided density (g cm^{-3})	Apparent porosity (%)	M.O.R. (MPa)
15 NBSN	1450/2	15	60.5	87.3	20.1	2.060	32.3	57 ± 10
25 NBSN	1450/4	25	60.9	79.4	29.1	2.123	30.5	78 ± 19
25 NBSNF[a]	1400/2	25	59.1	92.3	33.3	2.149	31.7	74 ± 16
50 NBSNF[a]	1400/2	50	59.7	93.9	59.6	2.279	26.8	147 ± 34

[a]1 wt.% of Fe_2O_3 addition with respect to silicon content.

$ percentage theoretical density with respect to the theoretical density of Si + Si_3N_4 mixtures calculated by the rule of mixtures (theoretical density for Si = 2.22 g cm^{-3} and for Si_3N_4 = 3.2 g cm^{-3}).

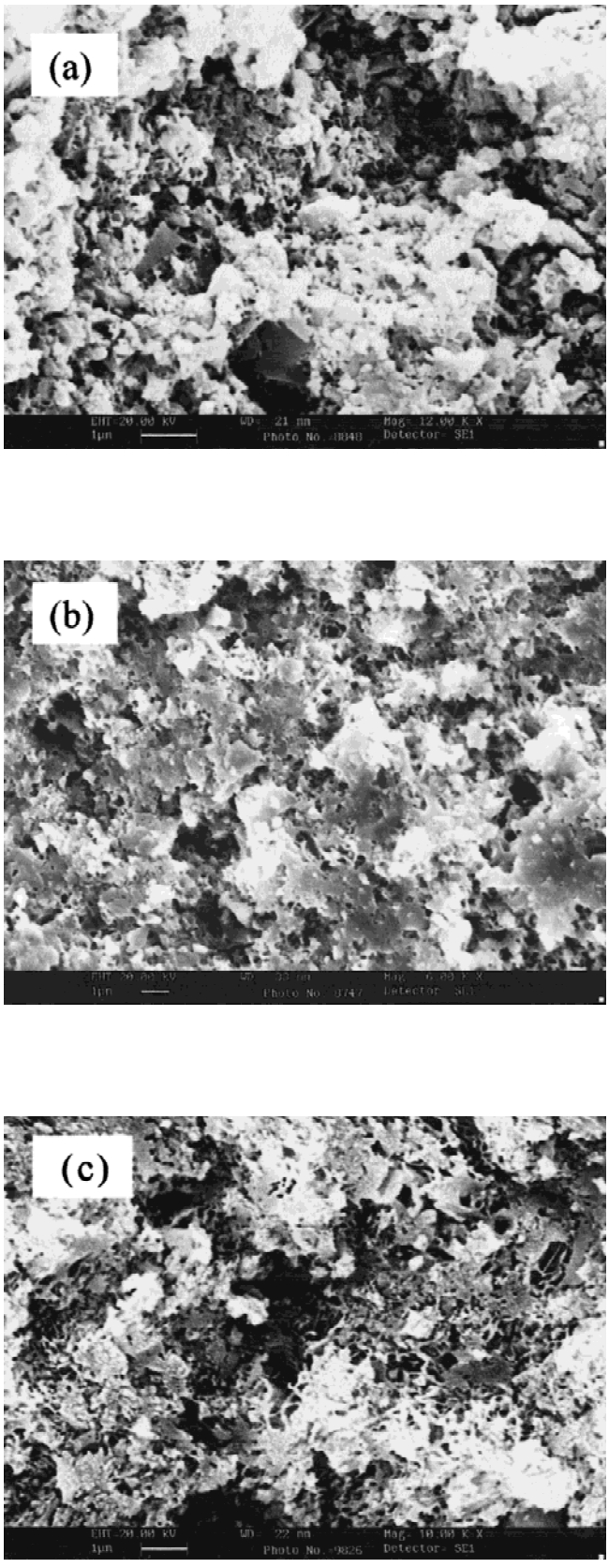

FIG. 9. Scanning electron micrographs of fractured surfaces of nitride-bonded silicon nitride products (a) 25 NBSNF, (b) 50 NBSNF, and (c) 50 NBSNF.

the α form and occasionally the β form. The predominant formation of α–Si_3N_4 is revealed clearly by XRD patterns of the nitrided products as presented in Figs. 8(b)–8(c) and is attributed to the seeding effect of the α–Si_3N_4 present in the starting Si + Si_3N_4 mixtures.[7,11–14] In comparison with the microstructure of the NBSC products[23,25] the microstructure of the NBSN products are more homogeneous with finer grain sizes, which could account for the good mechanical strengths observed in the later case.

IV. CONCLUSIONS

The optimum dispersion condition for Si and Si_3N_4 powders in aqueous media could be determined by employing various experimental techniques like particle-size analysis, sedimentation, viscosity, and ZP measurements as a function of pH of the medium. Based on the results of the above diagnostic tools, pH values of 8 to 10 were used for slip-casting Si + Si_3N_4 mixtures in various proportions in plaster molds to yield high-green density products with homogeneous microstructures. The nitridation experiments have proved that the extent of nitridation is a function of temperature, of time, and of the mass of Si present in the mixtures of Si + Si_3N_4 to be nitrided. Compacts with a higher percentage of Si nitrided to lower levels, those with lower percentage of Si nitrided to higher levels. The binding phase is most likely to be α–Si_3N_4 with a little of β–Si_3N_4 due to the self seeding effect by the higher percentage of α–Si_3N_4 phase present in the starting powder mixture. The NBSN products having 20% to 60% of Si_3N_4 bond show typical 3-point flexural strength values in the range 57 to 147 MPa despite their density lying in the lower range of 2.06 to 2.28 g cm^{-3}. The microstructure studies reveal a homogeneous distribution of different phases in the NBSN bodies, which have contributed considerably to the higher mechanical strength of these products.

ACKNOWLEDGMENTS

The authors gratefully acknowledge Dr. Kalyani Vijayan and Mrs. Anjana Jain for XRD spectra, Mr. M.A. Venkataswamy and Mrs. Kalavathi for SEM studies; Mr. A. Cheluvaraju, Miss H.N. Roopa, and Miss N. Shobha for assistance in slip casting and nitridation experiments. The authors would like to acknowledge the sustained encouragement given by Dr. R.V. Krishnan, Head, Materials Science Division, NAL, Bangalore during the course of these studies.

REFERENCES

1. R.N. Katz, in *Structural Ceramics, Treatise on Materials Science and Technology,* edited by J.B. Wachtman, Jr. (Academic Press, New York, 1989), Vol. 29, p. 1.

2. K. Komeya and M. Matsui, in *Materials Sciene and Technology, A Comprehensive Treatment*, edited by R.W. Cahn, P. Haasen, and E.J. Kramer, Vol. 11, Structure and Properties of Ceramics, Volume Ed., M.V. Swain (VCH Publishers, Weinheim, Germany, 1994), p. 517.
3. F.L. Riley, J. Am. Ceram. Soc. **83,** 245 (2000).
4. G. Woetting, G. Leimer, H.A. Lindner, and E. Gugel, Indus. Cer. **15,** 191 (1995).
5. G. Ziegler, J. Heinrich, and G. Woetting, J. Mater. Sci. **22,** 3041 (1987).
6. M.E. Washburn and W.S. Coblenz, Am. Ceram. Soc. Bull. **67**, 356, 360 (1988)
7. R.M. Williams and A. Ezis, Am. Ceram. Soc. Bull. **62,** 607, 619 (1983)
8. R. Pompe and L. Hermansson, Sprechsaal. **115,** 1098 (1982).
9. L.K.L. Falk, G.L. Dunlop, and R. Pompe, Mater. Sci. Eng. **71,** 123 (1985).
10. L.K.L. Falk, R. Pompe, and G.L. Dunlop, J. Mater. Sci. **20,** 3545 (1985).
11. A. Atkinson, P.J. Leatt, and A.J. Moulson, J. Mater. Sci. **7,** 482 (1972).
12. O.J. Gregory and M.H. Richman, J. Mater. Sci. Lett. **3,** 112 (1984).
13. R.M. Williams, A. Ezis, and J.C. Caverly, J. Am. Ceram. Soc. **67,** C–64 (1984).
14. J-L. Huang, S-W. Chen, H-H. Lu, and W-H. Chan, Ceramics International. **22,** 27 (1996).
15. R. Bhat and S.K. Roy, in *Advanced Ceramics*, edited by P. Ramakrishnan (Oxford and IBH Publishing Co. Pvt. Ltd., New Delhi, 1992), p. 51.
16. R. Ramachandra Rao, H.N. Roopa, and T.S. Kannan, J. Eur. Ceram. Soc. **19,** 2763 (1999).
17. R. Ramachandra Rao, H.N. Roopa, and T.S. Kannan, Bull. Mater. Sci. **24,** 57 (2001).
18. R.G. Stephen and F.L. Riley, J. Eur. Ceram. Soc. **5,** 219 (1989).
19. L. Bergstrom and R.J. Pugh, J. Am. Ceram. Soc. **72,** 103 (1989).
20. Y.L. Li, Y. Liang, F. Zheng, K. Xiao, Z.Q. Hu, and T. Shun, J. Mater. Sci. Letts. **14,** 713 (1995).
21. M.D. Sacks and G.W. Scheiffele, Ceram. Eng. Sci. Proc. **6,** 1109 (1985).
22. R. Ramachandra Rao, H.N. Roopa, and T.S. Kannan, Ceramics International. **25,** 223 (1999).
23. R. Ramachandra Rao, H.N. Roopa, and T.S. Kannan, J. Eur. Ceram. Soc. **19,** 2145 (1999).
24. R. Ramachandra Rao, H.N. Roopa, and T.S. Kannan, J. Mater. Sci. Letters **15,** 1956 (1996)
25. R. Ramachandra Rao, Ph.D. Thesis, Mangalore University, Karnataka, India, (2001).